Surface Temperature Measurements of GTA Weld Pools on Thin-Plate 304 Stainless Steel

Accumulated data can be useful in the development and verification of welding thermal models

BY H. G. KRAUS

ABSTRACT. The optical spectral radiometric/laser reflectance method, previously developed by this author, was used to produce high-resolution surface temperature maps of quasi-steady-state GTA weld pools in 1.5-mm-thick AISI 304 stainless steel that was moving during welding. Both temperature contour maps and temperature topology plots were produced for welding powers from 38 to 100 A, with travel speeds from 0.423 to 4.230 mm/s (1 to 10 ipm), allowing dependencies on these parameters to be assessed. These measurements extend similar but less extensive measurements made previously, and allow effects of refinements in the experimental method to be assessed. Results show that peak weld pool temperatures range from 2050 to 2570 K (1770° to 2300°C).

Introduction

The optical spectral radiometric/laser reflectance method, previously developed by this author, (Refs. 1, 2) has been used to obtain more extensive measurements of gas tungsten arc (GTA) weld pool surface temperatures using thin-plate AISI 304 stainless steel. This method of temperature measurement requires the welding arc to be extinguished, immediately after which temperature measurements are made. The results reported here were made to assess the effect of decreasing the welding arc shut-off time by an order of magnitude over previous measurements (Ref. 3), from 25–30 ms to 2–4 ms. One of the cases was extrapolated back to a time of 0 ms (beginning of arc decay) to estimate the magnitude of the maximum weld pool temperature decrease during arc decay.

The purpose of this and future research is to build a data base for verification and further development of theoretical thermal models of weld pools using various welding conditions and different materials. This data base will include stationary and moving welding conditions. To date, measurements have included those described above, as well as thick-plate (1.25 cm/0.5 in.) stationary welds on materials such as AISI stainless steel 304 and 316L, and 8630 (Ref. 4). Different heats of some of the thick-plate materials have been used, which have small variations in minor alloying elements such as cerium, silicon and sulfur. This will aid in assessing the well-known effect of surface tension induced by centrally inward or outward pool surface circulation patterns on pool surface temperatures. Future plans are then to add to these measurements by including thick-plate moving welding measurements on 304, as well as sulfur- and selenium-doped 304. The former will include the effects of power and translation speed, while the latter will investigate surface-tension effects. However, in order to accurately make such measurements, an experimental method to map the weld pool surface topology, at the same instant as the temperature measurements are being made, needs to be developed.

Background

Several other methods have been used to obtain weld pool surface temperature measurements. They have been reviewed elsewhere (Refs. 2, 3). There is one additional significant work that needs to be identified by Sundell, *et al.* (Ref. 5).

KEY WORDS

Temperature Contours
Temperature Maps
Temperature Topology
Surface Temperature
GTA Weld Pools
Thin AISI 304 Steel
Arc Decay
Welding Thermal Model
Emissivity
Laser Reflection

This report is an extensive investigation into the effects of minor alloying elements on GTA weld penetration. Spot weld pool surface temperature measurements are reported, as well as extensive molten metal surface tension data for AISI 8630 low-alloy steel, 316L stainless steel and Inconel® 718. Previous weld pool surface temperature measurements are well summarized by stating that they are either low-resolution spot measurements or uncalibrated infrared map measurements. The measurement results given here are high-resolution, absolute-temperature maps of the weld pools (minus what is blocked from view by the electrode and its spectral reflection off of the weld pools).

Experimental Procedure

Details of the optical spectral radiometric/laser reflectance measurement method can be found elsewhere (Ref. 2). The basis for the method is the following equation:

$$T = \frac{C_2}{\lambda \ln\left[1 + \frac{(2C_1 \cos\beta)\epsilon'_\lambda(\lambda,\beta,T)}{\lambda^5 e'_\lambda(\lambda,\beta,T)}\right]} \quad (1)$$

which is based on Planck's blackbody spectral distribution of emissive power, the definition of spectral directional emissivity, and Lambert's cosine law of diffuse emitters (see Ref. 6 for definitions). In Equation 1, ϵ'_λ is the spectral directional emissivity, e'_λ is the spectral directional emissive power, λ is wavelength, β is the angle from the normal vector to a surface, and C1 and C2 are constants (defined in Ref. 6). Note that in order to find the temperature at a point on the weld pool surface, only the spectral directional emissive power and the spectral directional emissivity must be measured. The

H. G. KRAUS is a Senior Engineering Specialist with Idaho National Engineering Laboratory, EG&G Idaho, Inc., Idaho Falls, Idaho.

smaller the point or spot on the weld pool, the better the temperature resolution. Figure 1 shows the experimental configuration for determining the spectral directional emissive power of the weld pool. High-speed cinematography was used to photograph the weld pool thermal emissions through a helium-neon (HeNe) laserline filter as the welding arc is extinguished, so as to have a spectral emission image of the weld pool immediately after arc emissions cease. The welding torch was held stationary while the plate was moved underneath. The moving stage was not stopped as in past measurements (Ref. 3) because the arc decay time was so short in the measurements reported here that the weld pool movement relative to the electrode is negligible. Filming speed was a critical parameter in obtaining useful information with respect to film image density. Controlled processing was used to develop the film, as well as using spectral sensitometry via a neutral-density step wedge (using also the same HeNe laserline filter) for recorded density (D) as a function of exposure (E). Figure 2 is an example of the film sensitometry curve for one of the runs described later, showing the film density at the head as well as the tail of the film roll. Film images were microdigitized for density using a 60-μm-square aperture having an image scale of the weld pool ranging from 1:1 to 1:1½ on 16-mm high-speed, red-sensitive Kodak 2484 film. The film density at each pixel is linearly interpolated between the head and the tail of the film based on the film footage number of the weld pool image immediately after arc emissions cease. Noise in the images, caused by grain clumping, was filtered out using a digital convolution filter. Calibration of the film image density was performed by matching the actual weld pool size to a particular film image constant-density contour at the phase front of the weld pool where the temperature is known (melting temperature of the metal). This temperature was assumed to be the average of the solidus and the liquidus temperatures for the alloy.

Equation 1 must be calibrated for absolute values of the spectral directional emissive power. Once spectral directional emissivity data are obtained, as explained below, they are used in conjunction with the known temperature of the phase front to calculate a constant factor, called the "wavelength constant," which is used to provide a calibration of the temperature equation, Equation 1. The wavelength constant is a system parameter that gives a relative indication of the radiation collection/recording efficiency at a given wavelength for the spectral directional emissive power. It depends on many things, including film type, filming speed, film processing, mir-

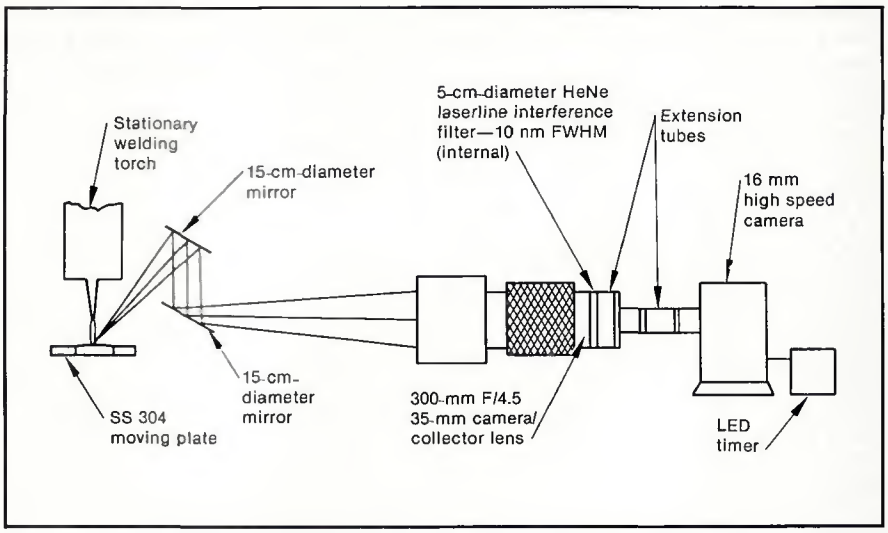

Fig. 1—Schematic for weld pool spectral directional emissive power experiment

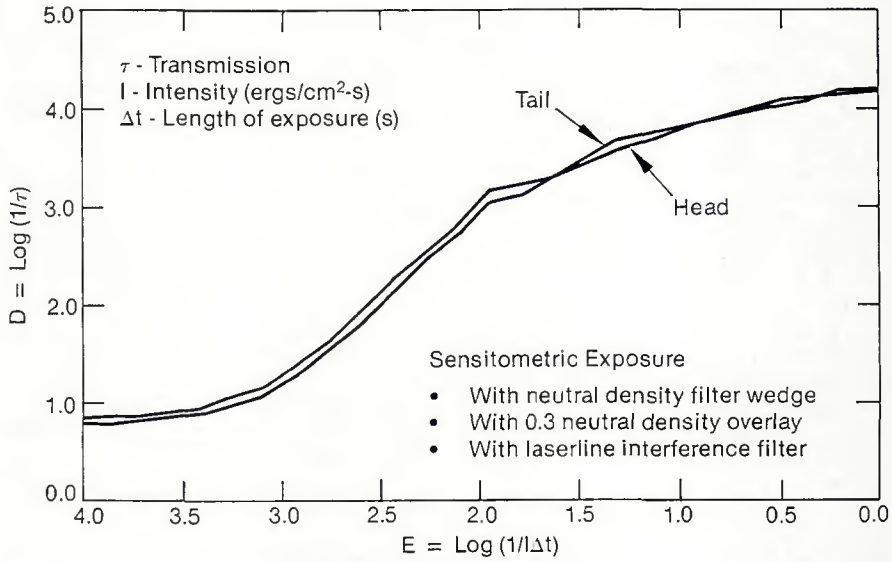

Fig. 2—Example spectral sensitometry (relative film calibration) curves—beginning and end of film roll

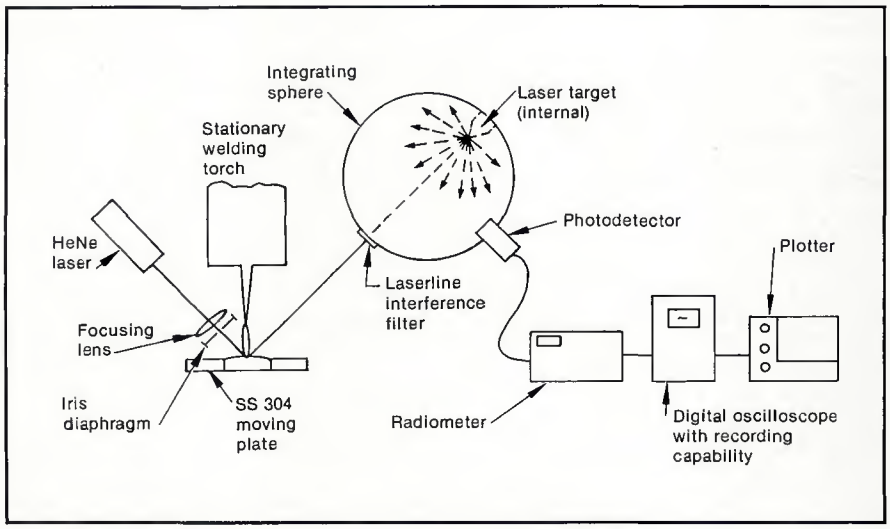

Fig. 3—Schematic for weld pool spectral directional emissivity experiment

Table 1—Conditions Summary of Type 304 Thin-Plate GTA Weld Pool Surface Temperature Measurement Runs with Maximum Temperature Results

Case No.	Welding Voltage (V)	Welding Current (A)	Travel Speed, mm/s (ipm)[a]	Time after Beginning of Emissions Decay (ms)	Maximum Observed Temperature K (°C)	Ratio of Welding Power to Travel Speed (W/(mm/s))
1	10.1	38	0.423 (1)	<3.6	2335 (2062)	907.3
2	10.1	38	0.423 (1)	0.0[b]	2273 (2000)	907.3
3	10.1	38	0.423 (1)	<3.6	2291 (2018)	907.3
4	10.1	38	0.423 (1)	<3.6	2332 (2059)	907.3
5	10.1	50	1.270 (3)	<3.6	2075 (1802)	397.6
6	10.1	50	1.270 (3)	<3.6	2259 (1986)	397.6
7	10.1	50	1.270 (3)	<3.6	2075 (1802)	397.6
8	10.1	50	1.270 (3)	<3.6	2052 (1772)	397.6
9	10.1	70	2.540 (6)	3.6	2422 (2149)	278.3
10	10.1	70	2.540 (6)	3.6	2493 (2126)	278.3
11	10.1	70	2.540 (6)	3.6	2296 (2023)	278.3
12	10.1	70	2.540 (6)	3.6	2484 (2211)	278.3
13	10.1	100	4.230 (10)	3.6	2523 (2250)	238.8
14	10.1	100	4.230 (10)	3.6	2569 (2296)	238.8

(a) In all cases, the welding machine was run for 15 to 25 s before arc shutoff in order to insure that quasi-steady-state conditions had been reached.
(b) Back-extrapolated temperature. See text.

ror reflectivities, camera lens, laserline filter transmission characteristics, etc. However, it remains fixed for any particular system and a given film image. Density values at all film image pixels are then converted to absolute spectral directional emissive power values using sensitometry data and wavelength constant.

The spectral directional emissivity of Type 304 weld pools was measured as a function of location, and thus temperature, in previous research (Ref. 3). This was done by reflecting a focused helium-neon laser beam off of the weld pool and relating the spectral directional reflectivity to the spectral directional emissivity via Kirchoff's law as (Ref. 6)

$$\epsilon'_\lambda (\lambda,\beta,T) = 1 - \rho'_\lambda (\lambda,\beta,T) \qquad (2)$$

In this equation, ϵ'_λ is the spectral directional emissivity, and ρ'_λ is the spectral directional reflectivity. The experimental configuration for this experiment is given in Fig. 3. Measurements are made at the same point in time, *i.e.,* at the end of arc emissions decay where the emissive power measurements are made. The location of the beam on the weld pool surface then allows the association with temperature at that location to be made. Results reported by Kraus (Ref. 3) show that there is no discernible spectral directional emissivity temperature dependence for 304 stainless steel, and that it has a value of 0.41 ± 0.01.

Weld pool temperatures are finally determined via Equation 1 by using the spectral directional emissive power and emissivity data corresponding to each pixel on the 16-mm film frame. Note that Equation 1 requires the measurement of temperature at a pixel to be made using the same value of β for both the emissive power and the emissivity measurements at a pixel. Temperatures below the phase-change temperature are not determined. In the event that the emissivity was temperature dependent, a trial and error procedure would be required in Equation 1 to determine each pixel temperature because it is not known *a priori.*

The primary motivation for the research results reported here is to assess the effect of arc shutdown time on the weld pool surface temperatures resulting from GTA welds on 1.5-mm-thick 304 sheets. Previous welds (Ref. 3) were made using a Miller Syncrowave 300 welding machine with a ⅛-in., 30-deg cone angle, 2% thoriated, tungsten electrode. The electrode gap was 1.5 mm. Argon cover gas with a flow rate of 18 cfph was used. The welds were run for 15–25 s to allow quasi-steady-state conditions to be reached. Upon shutting the welding machine off while the high-speed camera is running, the resulting arc decay times were 25–30 ms. For the results reported below, an Astro Arc Astromatic E-300-PC welding machine was used with the same configuration electrode, cover gas and cover-gas flow rate. However, in the latter case, the arc decay times were reduced to 2–4 ms. With the reduced arc decay times, it is believed that these new measurements would more closely represent the temperatures that exist when the arc is on. An estimate of the change in maximum weld pool temperature during arc shutoff was made. The Astro Arc results will first be reported and then compared to results from previous work.

Results

Table 1 summarizes the conditions for which new weld pool surface temperature maps have been made. With the welding voltage constant at 10.1 V, the current was varied from 38 to 100 A while the welding travel speed (actually the plate travel speed in this case since the welding torch was held constant) was varied from 1 to 10 ipm. The filming speed used was 280 fps, which results in a frame every 3.57 ms. In all cases, the arc decay period was in the range of 2 to 4 ms. (Detailed arc decay measurements were made for the Astro Arc power source in the above defined configuration in other research – Ref. 4.) This represents approximately one film frame, as reported in Table 1, for the arc emissions decay. Isothermal contour plots, as well as corresponding temperature topology plots, have been made for the first two welds of each welding current level in Table 1. These are shown in Figs. 4 through 11. Temperatures below the 1700 K melting temperature of 304 stainless steel are not shown. Also, the electrode and its spectral reflection, labeled in the isothermal contour plots, have fictitious temperatures because no attempt was made to measure the spectral directional properties of the electrode. The depression in the isotherms of Figs. 4 and 5 in the region of the electrode is caused by the cooler electrode temperature of the 38-A runs compared to the runs of higher welding current. Note that as the current was increased from 38 to 100 A in Figs. 4 through 11, this region of the electrode increases in temperature. Removal of the electrode and its reflection followed by temperature contour fill-in is possible; however, this was not done because there was no way to assure that these would represent the temperatures that actually existed. Maximum weld pool surface temperatures range from 1770° to 2300°C. The uncertainty of these measurements is believed to be ± 1–2%, or ± 25–50 K, based on a previous analysis of sources of error involved (Ref. 2).

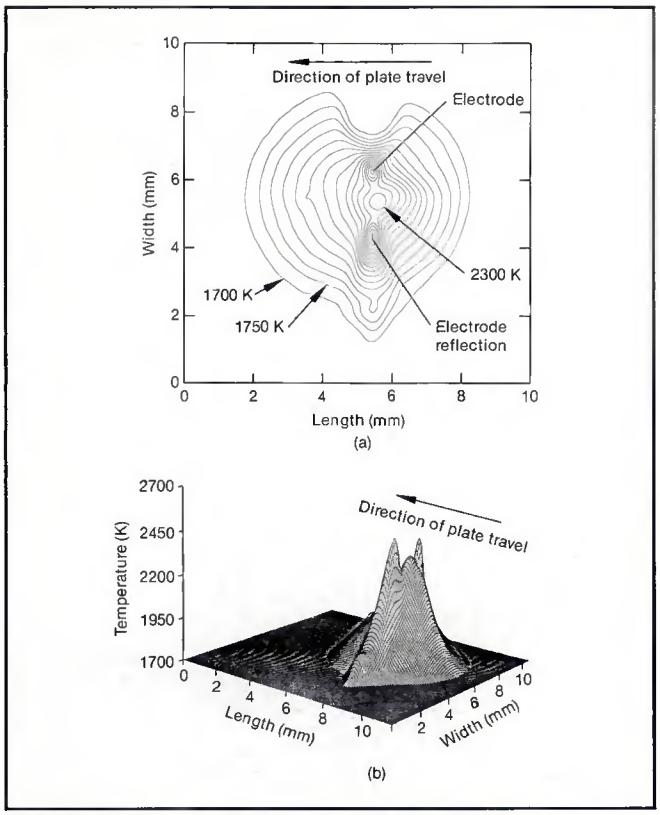

Fig. 4 — Weld pool surface. A — Isothermal temperature contours; B — temperature topology for thin-plate 304 stainless steel, 10.1 V, 38 A, 0.423 mm/s (Case 1 of Table 1)

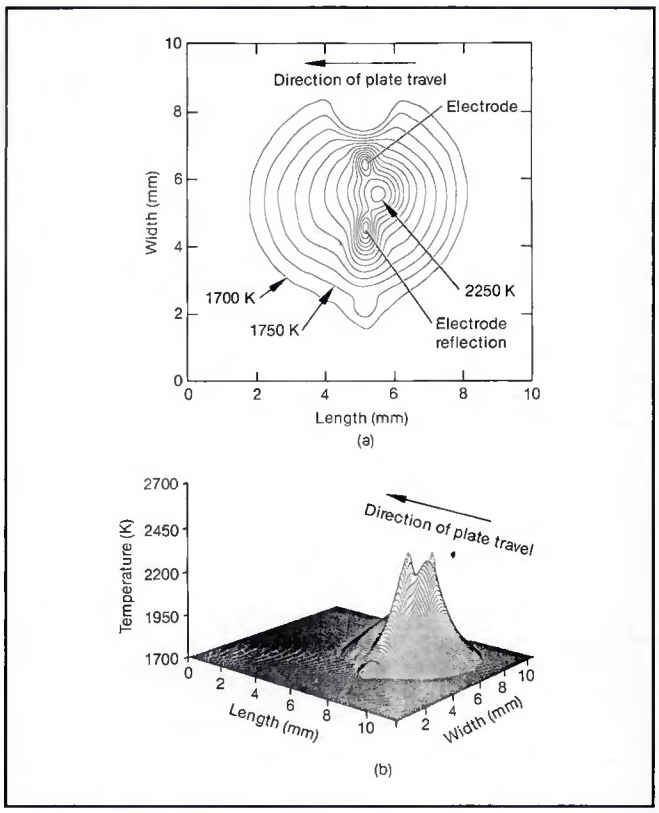

Fig. 5 — Weld pool surface. A — Isothermal temperature contours; B — temperature topology for thin-plate 304 stainless steel, 10.1 V, 38 A, 0.423 mm/s (Case 2 of Table 1)

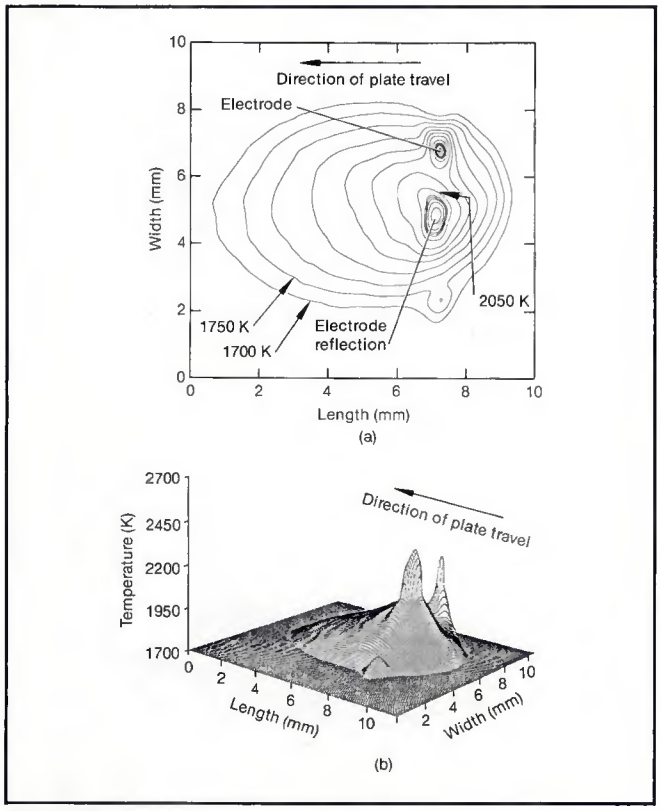

Fig. 6 — Weld pool surface. A — Isothermal temperature contours; B — temperature topology for thin-plate 304 stainless steel, 10.1 V, 50 A, 1.27 mm/s (Case 5 of Table 4)

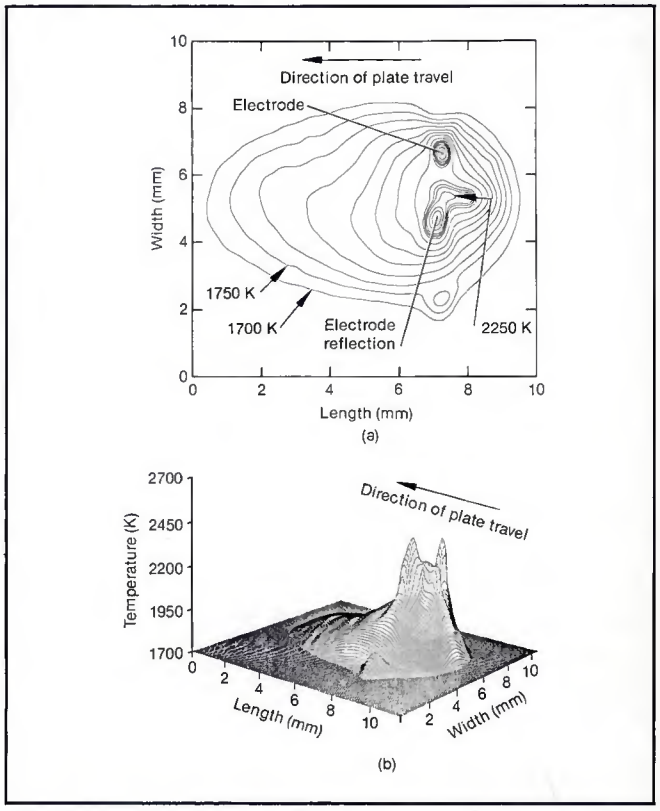

Fig. 7 — Weld pool surface. A — Isothermal temperature contours; B — temperature topology for thin-plate 304 stainless steel, 10.1 V, 50 A, 1.27 mm/s (Case 6 of Table 1)

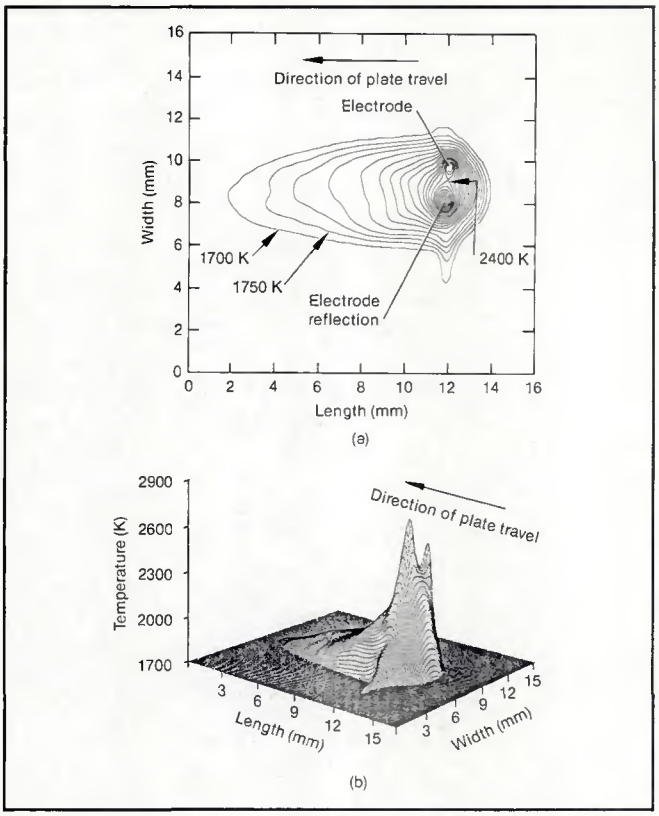

Fig. 8 — Weld pool surface. A — Isothermal temperature contours; B — temperature topology for thin-plate 304 stainless steel, 10.1 V, 70 A, 2.54 mm/s (Case 9 of Table 1)

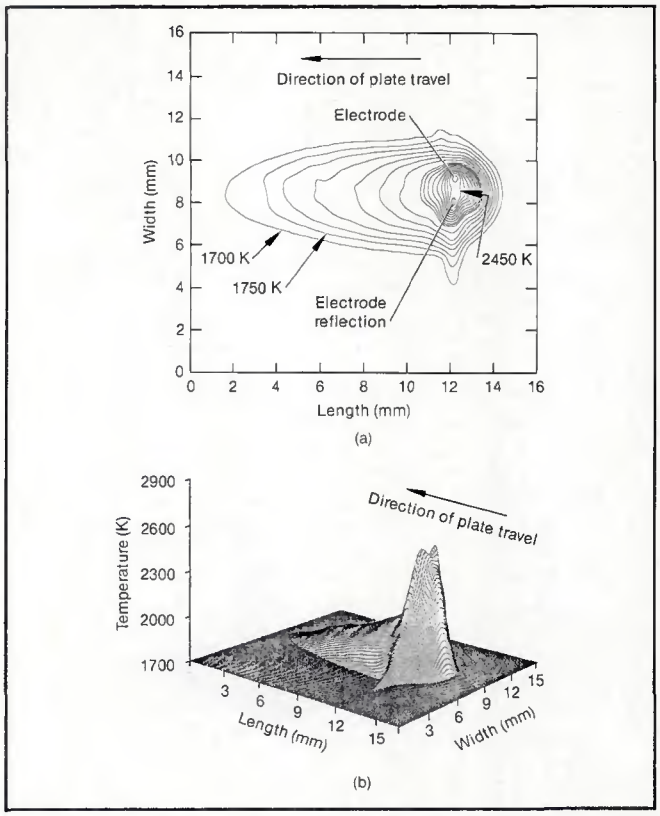

Fig. 9 — Weld pool surface. A — Isothermal temperature contours; B — temperature topology for thin-plate 304 stainless steel, 10.1 V, 70 A, 2.54 mm/s (Case 10 of Table 1)

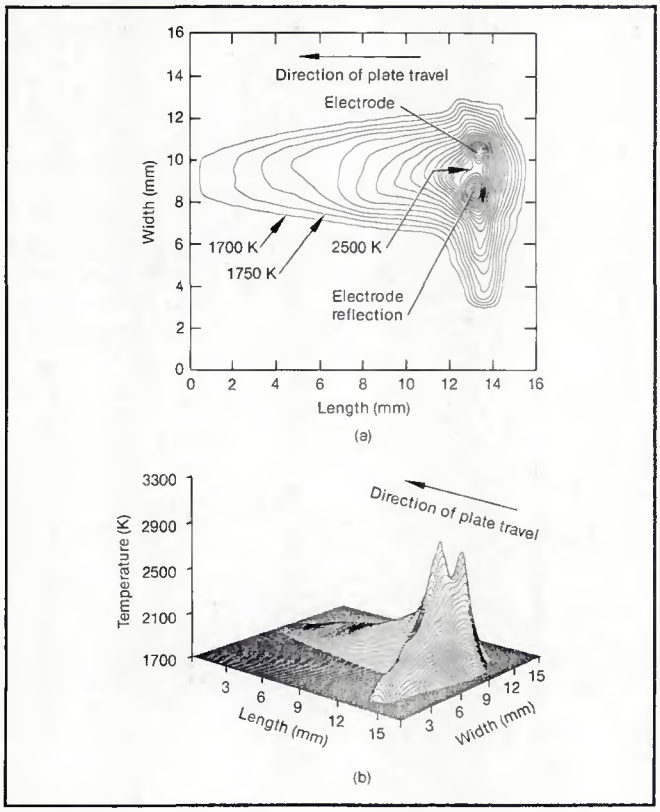

Fig. 10 — Weld pool surface. A — Isothermal temperature contours; B — temperature topology for thin-plate 304 stainless steel, 10.1 V, 100 A, 4.23 mm/s (Case 13 of Table 1)

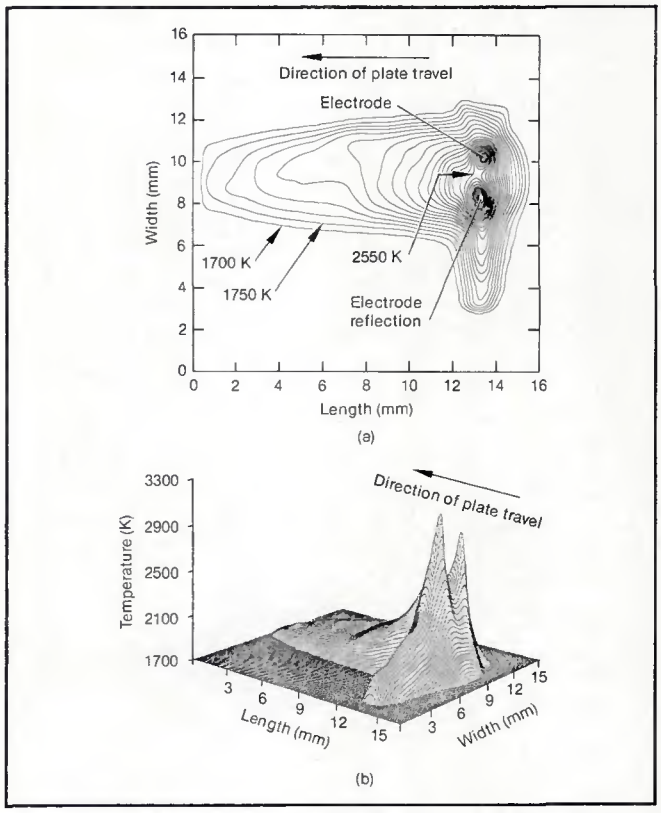

Fig. 11 — Weld pool surface. A — Isothermal temperature contours; B — temperature topology for thin-plate 304 stainless steel, 10.1 V, 100 A, 4.23 mm/s (Case 14 of Table 1)

The dependence of maximum weld pool temperature on welding power and travel speed can best be examined by looking at the ratio of welding power to welding speed as tabulated in the last column of Table 1. As this ratio decreases from 907 to 398 to 278 to 239, the group average (those of the same welding current) peak weld pool temperatures change from 2035° to 1840° to 2130° to 2270°C (see also Table 2). Thus, the welding power/welding speed ratio, which is a measure of the rate of energy input over the workpiece surface, does not produce the expected proportional relationship to maximum surface temperature. Rather, as this ratio is initially decreased, peak temperature decreases and passes through a minimum surface temperature—further decreasing this ratio causes the maximum temperature to increase. It is not believed that arc efficiency, which is well known to be relatively constant with welding current, is the explanation for this. The explanation is believed to lie in the changing weld pool convective characteristics, which have not been investigated for thin-plate welds.

A comparison of the average maximum weld pool surface temperatures for above results and previous welding results (Ref. 3) is made in Table 2. The corresponding translation speeds at each current level are the same as those shown in Table 1. Note that while the maximum temperatures for the 50-A and 70-A cases increased 40° and 220°C, respectively, those for the 38-A case decreased 495°C. Previous measurements using the Miller power source were not made at 100 A. This indicates that there are factors other than just the arc shutdown time that affect these measurements. Table 2 does show some power level differences, but the resulting trends are not consistent, *i.e.*, peak temperatures do not always increase with increasing welding power. Other possible explanations include specific power source characteristics, possibly affecting power delivery through the arc, arc argon plasma characteristics, and material composition differences. Chemical composition of the different heats of 304 used in these experiments are given in Table 3. Previous research (Refs. 5, 7, 8) has shown that minor alloying elements such as cerium, silicon and sulfur can have significant effects on weld pool shape and penetration, and presumably surface temperatures, for thick-plate welds. Even though there is a significant difference in the amount of sulfur in the two heats of Type 304 in Table 3, no significant difference was seen in the size of the resulting welds on the two different heats at a given amperage level. There are insufficient data here to explain the Table 2 results and such was not the goal of the present research. Further research would be needed to fully explain these results. However, it is believed that the decrease in arc shutdown time from 25–30 ms to 2–4 ms does allow these measurements to better represent temperatures present on the surface of the weld pools immediately before welding arc is extinguished.

Table 2—Comparison of Effect of Arc Shutdown Time on Average Maximum 304 Thin-Plate Weld Pool Surface Temperatures

Voltage (V)	Current (A)	Avg. T_{max} (°C) Arc Decay of 25–30 ms[a]	Avg. T_{max} (°C) Arc Decay of 2–4 ms
8.0	38	2530	
10.1	38		2035
8.25	50	1800	
10.1	50		1840
8.375	70	1910	
10.1	70		2130
10.1	100		2270

(a) Data from Ref. 3.

Table 3—Chemical Composition of 304 Thin-Plate Heats

Element	Heat A (Previous) wt-%	Heat B (Present) wt-%
C	0.1	0.06
Co	N/A	0.210
Cr	17.52	18.13
Cu	N/A	0.17
Fe	remainder	remainder
Mn	1.6	1.68
Mo	0.28	0.29
N	N/A	N/A
Ni	7.75	8.49
P	0.039	0.035
S	0.015	0.007
Si	0.5	0.55
V	0.051	0.055

The peak weld pool temperature results reported above, which average 2040°C (2313 K), compare well to the electron beam 304 stainless steel peak weld pool results of 2100°C (2373 K) by Shauer, *et al.* (Ref. 9); the 2000°C (2273 K) peak stationary 304 stainless steel weld pool measurements by Giedt, *et al.* (Ref. 10); and the vaporization theory based calculations of 2010°C (2283 K) for 10% of the workpiece input energy going into metal vaporization by Block-Bolten and Eagar (Ref. 11). True vaporization losses are probably between 1 and 10% (Ref. 11). More recently, Sundell, *et al.* (Ref. 5), made spot measurements of weld pool temperatures and found a peak of 1810°C (2083 K) for GTA welds on Type 304, ¾-in. (19-mm) thick plate using 250 A and a 3-ipm travel speed.

It is still appropriate to ask the question as to how much does the temperature of the weld pool decrease during the 2–4 ms of arc decay in the new measurements reported in this article. To aid in answering this question, the weld pool surface temperatures corresponding to the second 38-A run of Table 1 were extrapolated back to a time of 0.0 ms. This was done by taking five successive frames, starting with the first frame at 3.6 ms (immediately after arc emissions cease) and extrapolating the data back to the beginning of arc decay. Figure 12 shows the maximum weld pool temperatures for the first 18 ms, in 3.6-ms intervals, as experimentally measured from the actual data of this run. To extrapolate back to a time of 0.0 ms, these data cannot simply be curve-fit, thus a time that equals 0.0 ms temperature cannot be calculated. This is because during arc decay, the arc is still adding energy to the

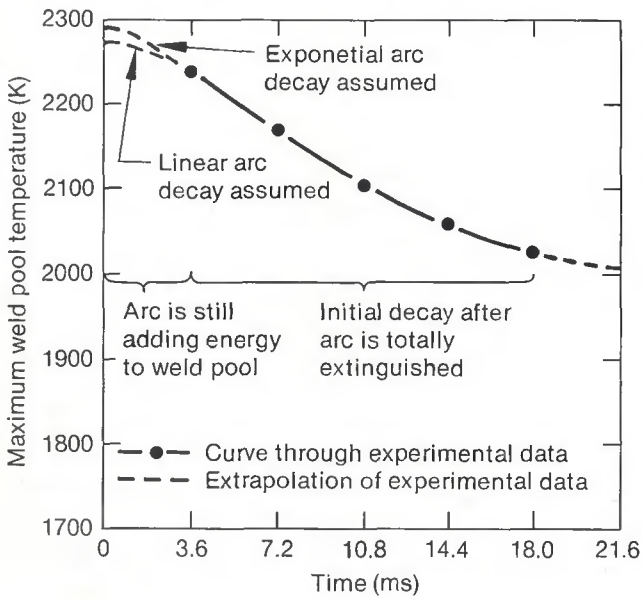

Fig. 12—Peak weld pool surface temperature as a function of time, beginning at the initiation of arc shutoff (Case 2 of Table 1)

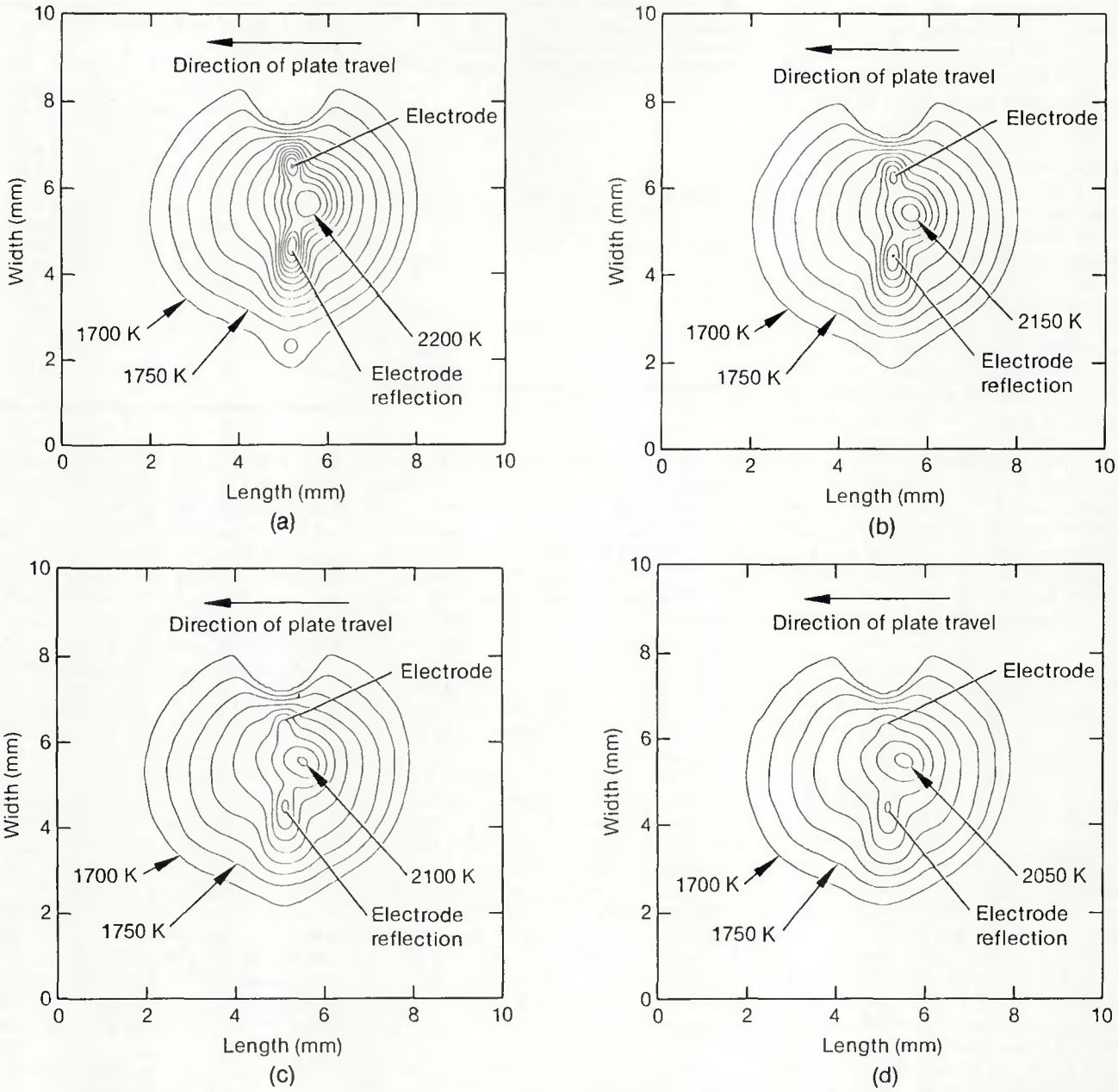

Fig. 13 — Weld pool surface isothermal temperature contour maps at: A — 7.2 ms; B — 10.8 ms; C — 14.4 ms; D — 18.0 ms into shutoff transient (Case 2 of Table 1). See Fig. 5A for 3.6 ms contours

weld pool. Detailed arc decay time measurements support the idea that the energy is being diverted away from the welding torch and cable at a linear rate as it dumps this energy to a large (20-kW) transistor diversion bank (Ref. 4). Such a back extrapolation could be reasonably assumed to give a temperature change during arc decay of ½ of that from 3.6 to 7.2 ms, or 35 K. This results in a maximum weld pool surface temperature of 2273 K as reported for a 0.0-ms decay time in the Table 1 results. This back extrapolation is shown in Fig. 12 as that for linear arc decay assumed. Although it is experimentally unsupported in this case because of the physical configuration of the Astro Arc power source for shutoff, if an exponentially decaying power curve were assumed (typical inductance/resistance decay), the input power to the welding machine can be easily shown to be no more than 25% of the power that would have been present during the 3.6-ms time interval if the machine had not been shut off. This assumes that a time equal to four time constants has passed, at which time arc decay energy input to the weld pool has decayed to <2% of its quasi-steady-state value. The decrease in maximum weld pool temperature would then have been ¾ of the 70 K drop from 3.6 to 7.2 ms, as shown in Fig. 12. In this case, a time 0.0 ms maximum weld pool temperature of 2292 K would have been predicted. This is represented by the upper extrapolated curve in Fig. 12 identified as exponential arc decay assumed. Finally, note that Fig. 5 represents the time 0.0 ms extrapolated temperatures of the entire temperature field and is consistent with the data reported in Table 1 for linear arc decay assumed. Here, back extrapolation was done by changing the film density calibration until the maximum weld pool surface temperature was equal to 2273 K. Linear arc decay is supported by experimental data and this results in about a 1.5% decrease in maximum weld pool temperature during arc decay. This is assumed to be applicable to all of the maximum temperature data of Table 1. Figure 13 shows the weld pool isothermal contours during the interval from 3.6 ms

to 14.4 ms after the initiation of arc decay for this 38-A run, and these correspond to the first four data points for maximum weld pool temperatures shown in Fig. 12. Figures 12 and 13 show that after arc shutoff, the initial rate of weld pool cooling in the region of maximum temperatures is quite rapid, but has slowed considerably by 20 ms into the shutoff transient.

Summary and Conclusions

The following statements summarize the findings of this research:

1) Detailed weld pool surface measurements have been made for 1.5-mm-thick SS 304 plates for welding currents of 38, 50, 70 and 100 A, and for welding speeds of 0.423 to 4.230 mm/s (1 to 10 ipm), respectively. Results showed that peak weld pool temperatures ranged from 2050 to 2570 K. Repeatability runs were made with run-to-run variation of 50° to 200°C. Maximum weld pool surface temperature was seen to decrease as the ratio of welding power to welding speed was decreased from 907 to 398. However, further decreasing this ratio results in increasing peak weld pool temperatures.

2) Comparing these results to previous results did not reveal that shorter arc decay shutdown times, in the experimental measurement procedure, will always result in higher measured temperatures.

3) While surface temperature maps of welds made under the same conditions have the same general characteristics, the temperature maps vary in their details. This is due to a phenomenon previously noted by this author that weld pool surface temperature profiles do not reach quasi-steady-state conditions, but rather vary around some time-averaged or mean values (Refs. 3, 4). Thus, successive temperature profiles, measured under the same welding conditions, vary predominately because of the particular instant when temperatures are observed during quasi-steady-state conditions.

4) The data reported here are intended to be used as part of a data base for theorists of welding processes to use for further development and verification of welding thermal models.

Acknowledgments

The author gratefully acknowledges Dr. H. B. Smartt for his continuing support of this research effort and L. D. Reynolds for assistance in the laboratory. The author would also like to thank J. H. Carson, J. J. Guenette and M. A. Lopez of EG&G Measurements, Los Alamos, N. Mex. for their aid in film processing and image microdigitizing.

This research was funded by the Office of Naval Research under contract No. N00014-85-F-0057. The author is employed at a Department of Energy research facility under contract number DE-AC07-76-ID01570.

References

1. Kraus, H. G. 1986. Optical spectral radiometric method for measurement of weld pool surface temperatures. *Optics Letters* 11(12): 773–775.

2. Kraus, H. G. 1987. Optical spectral radiometric/laser reflectance method for noninvasive measurement of weld pool surface temperatures. *Opt. Eng.* 26(12): 1183–1190.

3. Kraus, H. G. 1987. Experimental measurement of thin plate 304 stainless steel GTA weld pool surface temperatures. *Welding Journal* 66(12): 353-s to 359-s.

4. Kraus, H. G. 1988. Experimental measurement of stationary SS 304, SS 316L and 8630 GTA weld pool surface temperatures. Presented at the 1988 AWS Conference, New Orleans, La., and accepted for publication in the *Welding Journal.*

5. Sundell, R. E., *et al.* 1986. *Minor Element Effects on Gas Tungsten Arc Weld Penetration.* Report No. 86SRD013, submitted to National Science Foundation, General Electric Co., Schenectady, N. Y.

6. Seigel, R., and Howell, J. R. 1976. *Thermal Radiation Heat Transfer.* 2nd Edition, McGraw-Hill.

7. Heiple, C. R., and Roper, J. R. 1982. Mechanism for minor element effect on GTA fusion-zone geometry. *Welding Journal* 61(4): 92-s to 102-s.

8. Heiple, C. R., Roper, J. R., and Aden, R. J. 1983. Surface active element effects on the shape of GTA, laser and electron beam welds. *Welding Journal* 62(3): 72-s to 77-s.

9. Shauer, D. A., Giedt, W. H., and Shintaku, S. M. 1978. Electron beam welding cavity temperature distributions in pure metals and alloys. *Welding Journal* 57(5): 127-s to 133-s.

10. Giedt, W. H., Wei, X-C., and Wei, S.-R. 1984. Effect of surface convection on stationary GTA weld zone temperatures. *Welding Journal* 63(12): 376-s to 383-s.

11. Block-Bolten, A., and Eagar, T. W. 1984. Metal vaporization from weld pools. *Met. Trans. B.* 15B(9): 461–469.

WRC Bulletin 332
April 1988

This Bulletin contains two reports that characterize the mechanical properties of two different structural shapes of constructional steels used in the pressure vessel industry.

(1) Characteristics of Heavyweight Wide-Flange Structural Shapes
By J. M. Barsom and B. G. Reisdorf

This report presents information concerning the chemical, microstructural and mechanical (including fracture toughness) properties for heavyweight wide-flange structural shapes of A36, A572 Grade 50 and A588 Grade A steels.

(2) Data Survey on Mechanical Property Characterization of A588 Steel Plates and Weldments
By A. W. Pense

This survey report summarizes, for the most part, unpublished data on the strength toughness and weldability of A588 Grade A and Grade B steels as influenced by heat treatment and processing.

Publication of this Bulletin was sponsored by the Subcommittee on Thermal and Mechanical Effects on Materials of the Pressure Vessel Research Committee of the Welding Research Council. The price of WRC Bulletin 332 is $20.00 per copy, plus $5.00 for postage and handling. Orders should be sent with payment to the Welding Research Council, Suite 1301, 345 E. 47th St., New York, NY 10017.